

# Hepatic inflammation-fibrosis-cancer axis in the rat hepatocellular carcinoma induced by diethylnitrosamine

Yong-fang Ding<sup>1,2</sup> · Zhen-hui Wu<sup>3</sup> · Ying-jie Wei<sup>1,2</sup> · Luan Shu<sup>1,2</sup> · Yun-ru Peng<sup>1,2</sup>

Received: 17 November 2016 / Accepted: 1 February 2017 / Published online: 25 February 2017  
© Springer-Verlag Berlin Heidelberg 2017

## Abstract

**Purpose** Hepatocellular carcinoma (HCC) cases are closely associated with chronic inflammation and fibrosis which is known as hepatic inflammation-fibrosis-cancer (IFC) axis. The aim of this study is to elucidate the development characteristics of the rat HCC model based on IFC axis.

**Methods** The diethylnitrosamine (DEN)-induced rat HCC, which presents a stepwise histopathological progression that is similar to human HCC, was used to analyze the features of the different stages (inflammation, fibrosis, cancer). Rats were injected DEN at a dose of 30 mg/kg body weight twice a week for 11 weeks and the animals were observed until week 20. Time series sera and organ samples from the DEN animal model were collected to evaluate the dynamic changes.

**Results** It was found that serum biochemical indicators (AST, ALT, ALP, TP, T-BIL, IL-6, TNF- $\alpha$ ) from DEN-treated group were higher than that from control group. Fibrosis-related index in serum and live tissue were increased, respectively, from week 4 after DEN treatment. The expression of TGF- $\beta$ 1 and  $\alpha$ -SMA in DEN-treated group was higher than that in control group. JAK2/STAT3 signaling was significantly up-regulated in DEN-treated

group compared to that in control group. The histological examination confirmed that the hepatocarcinogenesis model was successfully established, and 100% of the animals in the DEN-exposed group developed liver tumors at 20 weeks. According to the pathological changes, the model characterized resulted in three stages: the inflammation stage (week 2–6), the fibrosis stage (week 8–12), and the HCC stage (week 14–20).

**Conclusions** The results suggested that the HCC development was associated with IFC axis. The serial progression of hepatocarcinogenesis was according to the sequence of hepatic inflammation, fibrosis and then hepatic tumor.

**Keywords** Hepatocellular carcinoma · Liver inflammation · Liver fibrosis · Inflammation-fibrosis-cancer (IFC) axis

## Introduction

Hepatocellular carcinoma (HCC) is one of the major malignant tumors in humans, representing the fifth most common cancer and the third cause of cancer-related deaths worldwide (Hernandez-Gea et al. 2013). The rising incidence of HCC is largely due to the emergence of hepatitis C virus (HCV) and hepatitis B virus (HBV) viral infection, the liver pathologies associated with obesity and chronic alcohol abuse (Li et al. 2014). There is an urgent need to understand how HCC develops in the disease liver.

Upon exposure to risk factors like HCV, HBV, obesity, diabetes, alcohol, injury-induced hepatic cells undergo inflammation driven by Kupffer cell, dendritic cell, and hepatic stellate cell (HSC) (Cubero 2016). Chronic inflammation and the associated regenerative wound-healing response are strongly linked to the development

✉ Yun-ru Peng  
pengyunru@126.com

<sup>1</sup> Affiliated Hospital of Integrated Traditional Chinese and Western Medicine, Nanjing University of Chinese Medicine, Nanjing 210028, People's Republic of China

<sup>2</sup> Jiangsu Province Academy of Traditional Chinese Medicine, Nanjing 210028, People's Republic of China

<sup>3</sup> Nanjing University of Chinese Medicine, Nanjing 210028, People's Republic of China

of fibrosis. And almost 80% of HCC cases are associated with chronic hepatitis and cirrhosis resulting from inflammation and fibrosis. HCC is the final stage of this process. Some scholars call this sequence the hepatic inflammation-fibrosis-cancer (IFC) axis (Elsharkawy and Mann 2007). Approaches to HCC prevention should therefore be focused on the underlying molecular mechanisms of IFC process.

To make advances in research in the prevention of HCC based on IFC axis, several experimental models have been developed to investigate the aspects of the pathogenesis and etiology. Due to the similarity to histological and genetic features of patients, diethylnitrosamine (DEN)-induced HCC model, is commonly used to imitate the process of hepatocarcinogenesis. In this study, the DEN-induced HCC model was used to, respectively, analyze the each stage of hepatic inflammation, fibrogenesis, and cancer. Time series sera and organ samples from DEN animal model were analyzed to evaluate the dynamic changes and discover biomarker candidates. This present study aims to reveal the development of hepatocarcinoma based on hepatic IFC sequence.

## Materials and methods

### Experimental animals

Animal experiments were performed in accordance with the Guide for the Care and Use of Laboratory Animals published by the US National Institutes of Health (Publication No. 85-23, revised 1996), and the study was approved by our Academy Animal Experimental Ethical Committee. Male Sprague–Dawley rats, weighing 150–180 g, were purchased from Sino-British Sippr/BK Lab Animal Ltd. (Shanghai, China). All animals were housed in stainless steel cages and maintained under a 12 h:12 h light/dark cycle with constant temperature and humidity, and allowed free access to standard rat-chow diet and tap water. Animals were allowed a 1-week acclimatization period prior to the experimental protocol.

### Experimental design

The rats were randomly divided into two groups of ten rats for control group and 70 rats for DEN group. Control group was intraperitoneally injected with 0.9% normal saline solution twice a week. Model group was injected DEN (Sigma Aldrich, St. Louis, MO) at a dose of 30 mg/kg body weight (bw) on the same day as control group for 11 weeks (Zeng et al. 2015; Peng and Ding 2015). DEN was stopped then and the animals were observed until 20 weeks. Fourteen rats from the model group died during the administration. The experimental schedule is given in Fig. 1.

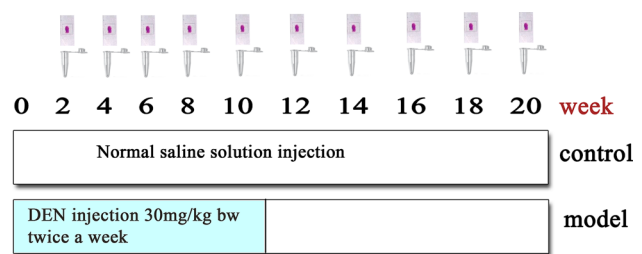


**Fig. 1** Experimental schedule

Body weight of the animals was measured once every 2 weeks throughout the study. To monitor the progress of stepwise hepatocarcinogenesis, a time-series sera set, including ten rats (11 rats in week 20) from DEN group and ten rats from control group, was collected once every 2 weeks from week 0 to week 20. Five rats from the model group were killed for histological examination every 2 weeks from week 2 to week 18. In week 20, all surviving rats ( $n=11$  for DEN group and  $n=10$  for control group) were finally killed. Collected liver tissues were weighted, and then fixed in 10% formalin for histopathology and immunohistochemical examinations. The remaining portion was kept at  $-80^{\circ}\text{C}$  for further analysis.

### Determination of biochemical indicators

Blood samples were collected via orbital venous. Serum levels of alanine aminotransferase (ALT), aspartate transaminase (AST), alkaline phosphatase (ALP), total protein (TP), albumin (ALB), globulin (GLO) and total bilirubin (T-BIL) were tested using an automatic analyzer (C8000 Roche; Hoffmann-La Roche Inc, Switzerland). Serum levels of tumor necrosis factor- $\alpha$  (TNF- $\alpha$ ), interleukin 6 (IL-6) were measured using ELISA kits (R&D Systems, Inc.), according to the manufacturer's instructions.

### Evaluation of fibrosis-related index

Serum liver fibrosis markers hyaluronic acid (HA), laminin (LN), procollagen III N-terminal peptide (P-III-NP) and collagen type IV (IV-C) were determined using radioimmunoassay (Beijing North Institute of Biological Technology, Beijing, China). As an indicator of total collagen content, hepatic hydroxyproline (Hyp) content was measured using ultraviolet spectrophotometry with the Hydroxyproline Assay kit (Nanjing Jiancheng Institute of Bioengineering, Nanjing, China) according to the manufacturer's instruction. Hyp content was expressed as  $\mu\text{g/g}$  of liver wet weight.

**Magnetic resonance imaging (MRI) analysis**

To monitor tumor growth, MR imaging was performed at 16th week, 18th week and 20th week. The animals were anesthesia using isoflurane, which was initiated in an induction chamber using a mixture of 4% isoflurane and 96% oxygen, and maintained with the mixture of 2% isoflurane and 98% oxygen at a flow rate of 0.8 L min. An 1.5-T whole-body MR imager (Sonata; Siemens, Erlangen, Germany) with a wrist coil was used to acquire T2-weighted MR images (T2WI, repetition time, 3000 ms; echo time, 57 ms; flip angle, 140°; field of view, 100×100 mm; matrix, 205×256; section thickness, 1.5 mm) (Li et al. 2011; Tyler et al. 2013).

**Histologic and immunohistochemical evaluation**

For assessment the pathological changes of the different stages about inflammation, fibrosis and carcinoma, livers were fixed in formaldehyde neutral buffer solution and cut into 4 μm sections. The hematoxylin–eosin (HE) staining and collagen-specific Masson staining were used for histopathological examination. Grading of inflammatory activity and staging of fibrosis were performed according to the METAVIR scoring system, a histological scale used to quantify the degree of inflammation and fibrosis. “A” refers to the intensity of necrosis and inflammation and may vary from A0 to A3 (A0=no activity, A1=mild activity, A2=moderate activity, and A3=severe activity). “F” refers to the extent of fibrosis and may vary from F0 to F4 (F0=no fibrosis, F1=portal fibrosis without septa, F2=portal fibrosis with rare septa, F3=numerous septa without cirrhosis, and F4=cirrhosis) (Knodell et al. 1981; Costentin et al. 2011). The development of HCC was studied by two independent pathologists who were blind to the study.

Immunohistochemical analyses of TGF-β<sub>1</sub> and α-SMA were performed using paraffin-embedded sections. The slides were incubated with antibody TGF-β<sub>1</sub> (1:100, ab92486, Abcam, UK) or α-SMA (1:100, ab5694, Abcam, UK) to detect bound antibodies. After staining, the sections were counterstained with hematoxylin for microscopy

analyses. All sections were examined by light microscopy (Axioskop 2 microscope, Carl Zeiss, Germany). The number of positive hepatocytes in liver specimens from each rat was counted in five random fields at 100× magnification. The percentage of positive area was determined using Image-Pro Plus 6.0 (Media Cybernetics Inc., Baltimore, MD, USA). The image analysis was conducted by pathologists blinded to the treatments.

**Western blotting analysis**

Western blotting procedures were performed as described previously with minor modifications (Ding et al. 2013). In brief, proteins were extracted from frozen liver tissues in 500 μl of RIPA Lysis buffer containing 1 mM PMSF. The protein level was measured by Bradford assay. Equal quantities of proteins (40 μg) were separated by 10% SDS-PAGE and transferred to PVDF membranes. Membranes were blocked and probed overnight at 4°C with polyclonal anti-TGF-β<sub>1</sub> (1:1000, ab92486, Abcam, UK), α-SMA (1:1000, ab5694, Abcam, UK), JAK2 (1:1000, ab39636, Abcam, UK), STAT3 (1:1000, ab68153, Abcam, UK) and P-STAT3 (1:2500, ab76315, Abcam, UK). After washing, the membranes were incubated for 1 h at room temperature with secondary antibody and visualized using ECL detection kit (KeyGEN BioTECH, China). Target proteins levels were normalized against the level of β-actin.

**RNA extraction and quantitative real-time PCR detection**

Total RNA was extracted from frozen liver tissues of rats using Trizol reagent and first-stand cDNA was produced using Thermo Fisher K1622 first-stand cDNA Synthesis Kit (Thermo Fisher, USA). Gene-specific primer sequences were designed using Primer 5.0 software and synthesized by GenScript Inc., Nanjing, China. The primer sequences utilized are shown in Table 1.

The PCR reaction was carried out in 20 μl reaction mixture containing 10 μl real-time PCR Master Mix (SYBR Green), 1 μl cDNA, and 2 μl primer mix (including forward and reverse primers) diluted in Rnase-free water. Relative

**Table 1** Primer sequences of target genes

Gene	Forward primer	Reverse primer
Collagen I	5-CTGCTGGTCCTAAGGGAGAG-3	5-GACAGCACCATCGTTACCAC-3
Collagen III	5-TCCTGGATACCAAGGTCCTC-3	5-GACCAATAGCACCAGGAGGT-3
α-SMA	5-GGGATCCTGACCCTGAAGTA-3	5-CACGCGAAGCTCGTTATAGA-3
TGF-β1	5-CTTGCCCTCTACAACCAACA-3	5-CTTGCGACCCACGTAGTAGA-3
IL-6	5-AAGGACCAAGACCATCCAAC-3	5-ACCACAGTGAGGAATGTCCA-3
TNF-α	5-AAACACACGAGACGCTGAAG-3	5-ATCCAGTGAGTCCGAAAGC-3
GAPDH	5-GGCCTTCCGTGTTCTACC-3	5-CGCCTGCTTACCACCTTC-3

gene expression was analyzed using the comparative  $\Delta\Delta C_t$  method with GAPDH (Duan et al. 2014).

### Statistical analysis

The obtained data were analyzed and using the statistical package for social science (SPSS, Version 11.5, SPSS Inc., Chicago, IL, USA). Data were presented as mean  $\pm$  SD. One-way analysis of variance (ANOVA) with LSD multiple comparison test was used for comparisons among all groups. The Kruskal–Wallis  $t$  test was used to compare the METAVIR score.  $P$  values  $<0.05$  were considered significant.

## Results

### General appearance and serum parameters

During the administration of DEN, 14 rats from the model group died of liver function failure. Body weight in the model group was lower than that in the control group at various time points ( $P < 0.01$ ). Average body weights of different groups are shown in Fig. 2. Final absolute and relative liver weights of model group were significantly increased as compared to those of the control group ( $P < 0.01$ ). Final

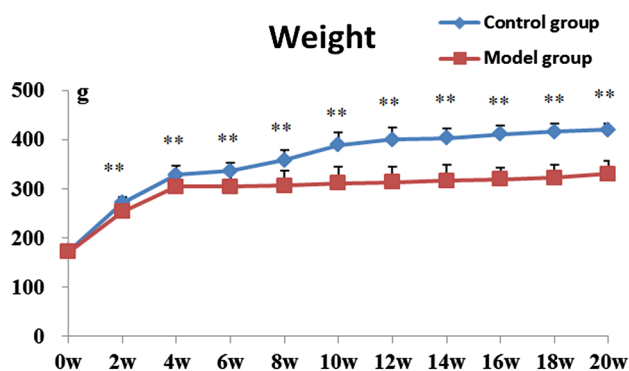


**Fig. 2** Growth curve of rats treated with diethylnitrosamine. Results are expressed as mean  $\pm$  SD ( $n = 10$ – $11$ ). \*\* $P < 0.01$  vs control group

**Table 2** Final body and liver weights of rats treated with diethylnitrosamine

Group	$n$	Final body weight (g)	Liver weight	
			Absolute (g)	Relative (/100 g bw)
Control group	10	419.6 $\pm$ 13.5	9.149 $\pm$ 0.976	2.179 $\pm$ 0.209
Model group	11	330.3 $\pm$ 27.3**	30.049 $\pm$ 2.705**	9.167 $\pm$ 1.218**

Values are expressed as the mean  $\pm$  SD

Relative liver weight = [liver weight (g)/body weight (bw,g)  $\times$  100]

\*\* $P < 0.01$  vs control group

body weights and absolute and relative liver weights of two groups are presented in Table 2.

Serum transaminase (ALT and AST) and ALP levels were higher in the DEN group and remained at a high level until the end of the experiment ( $P < 0.01$ ), which most likely reflected the hepatic injury induced by DEN (Fig. 3a–c). Serum TP level was higher in the DEN group compared to the control group from week 12 to week 20 ( $P < 0.05$ – $0.01$ , Fig. 3d). Serum T-BIL level was also significantly higher in the model group than that in the control and remained at a high level throughout the experiment period ( $P < 0.01$ , Fig. 3h).

Serum IL-6 level in DEN group was obviously increased from week 6 and reached the peak at week 12 (Fig. 3i). Serum TNF- $\alpha$  level was higher in DEN group than in control group in week 4 and week 6 ( $P < 0.01$ ), but no significant differences were identified in other weeks (Fig. 3l).

### Fibrosis-related index in serum and liver tissue

Serum fibrosis markers HA, LN, P-III-NP and IV-C are showed in Fig. 4. A gradual increase of the HA, LN, P-III-NP and IV-C concentrations was observed from week 4. Serum levels of these were significantly higher compared with control group (Fig. 4a–d,  $P < 0.05$ – $0.01$ ). After beginning of treatment DEN, hepatic hydroxyproline (Hyp) content, an indicator of total collagen content, was high and statistically significant from week 4 to week 20 (Fig. 3e).

### Results of magnetic resonance imaging (MRI) analysis

To evaluate tumor development, MRI was performed at 16th week, 18th week and 20th week. The liver nodules were consistently hyper-intense on the T2-weighted image (T2WI). Tumors were demonstrated in 11/11 cases (100%) at week 20 (Fig. 5). The maximum tumor diameter was up to 2.3 cm. The number and size of nodules in different individuals were unbalanced and the hepatic nodules were diffusely distributed. There were cystic degeneration, necrosis and hemorrhage in some nodules, therefore tumor masses showed mixed intensity on T2WI.

**Fig. 3** Effect of DEN on serum biochemical indicators. Serum levels of **a** ALT, **b** AST, **c** ALP, **d** TP, **e** ALB, **f** GLO, **g** A/G, **h** T-BIL, **i** IL-6, **j** TNF- $\alpha$ . Results are expressed as mean  $\pm$  SD ( $n=10-11$ ). \* $P<0.05$ , \*\* $P<0.01$  vs control group

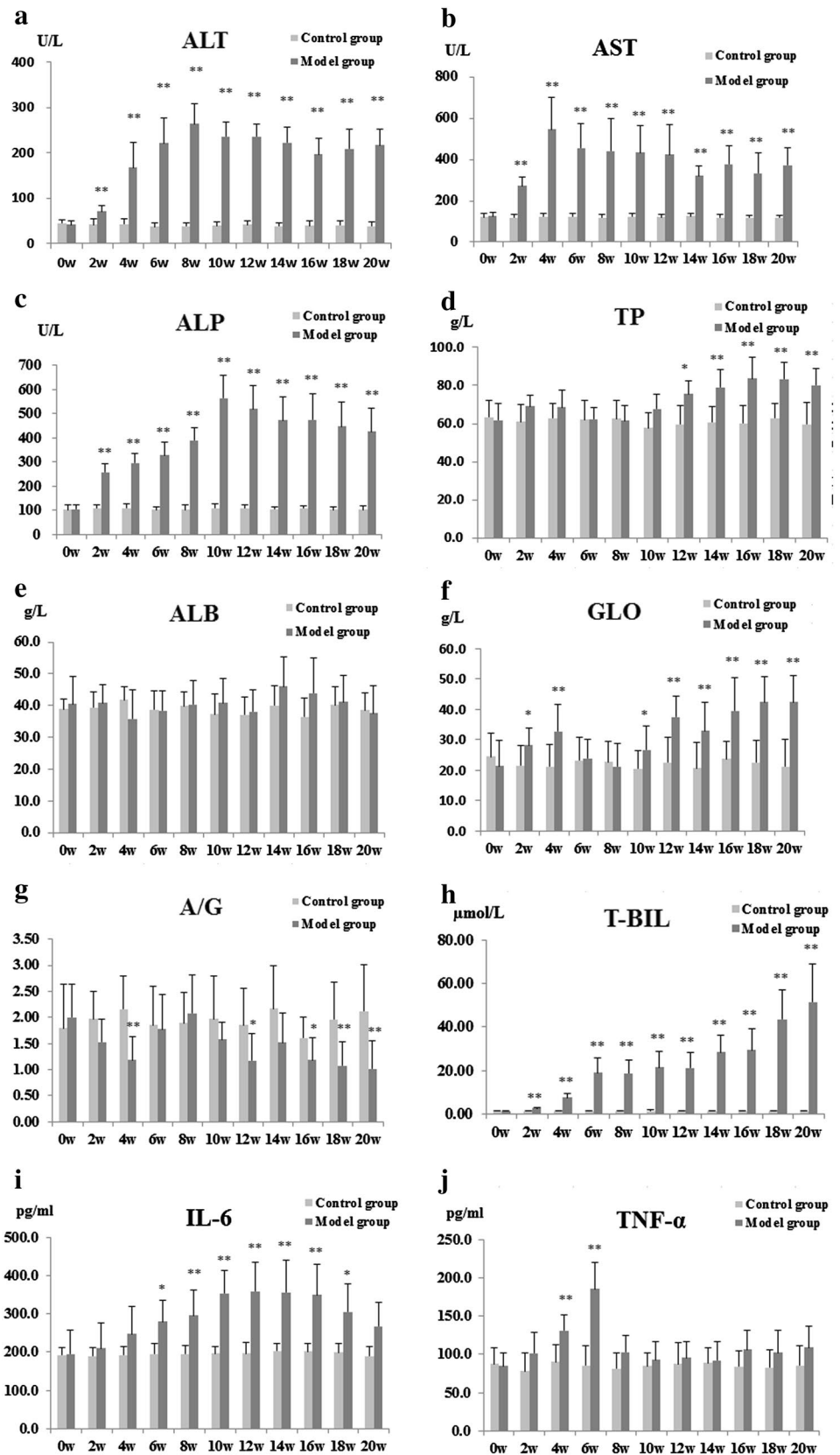


**Fig. 4** Effect of DEN on serum biochemical indicators. Serum levels of **a** HA, **b** LN, **c** P-IIIINP, **d** IV-C, and tissue level of **e** hydroxyproline. Results are expressed as mean  $\pm$  SD. ( $n=10-11$ ). \* $P<0.05$ , \*\* $P<0.01$  vs control group

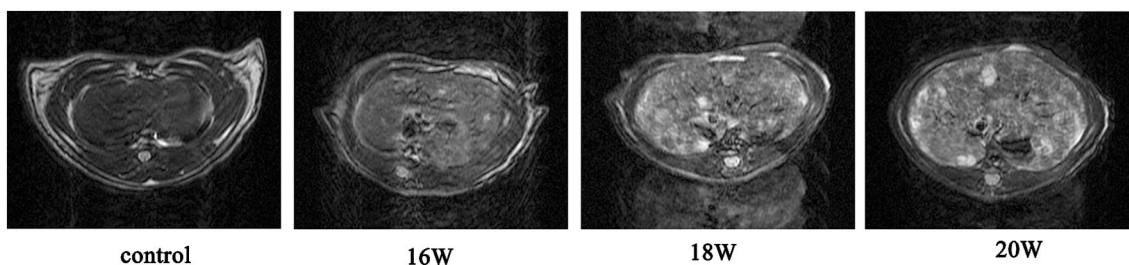
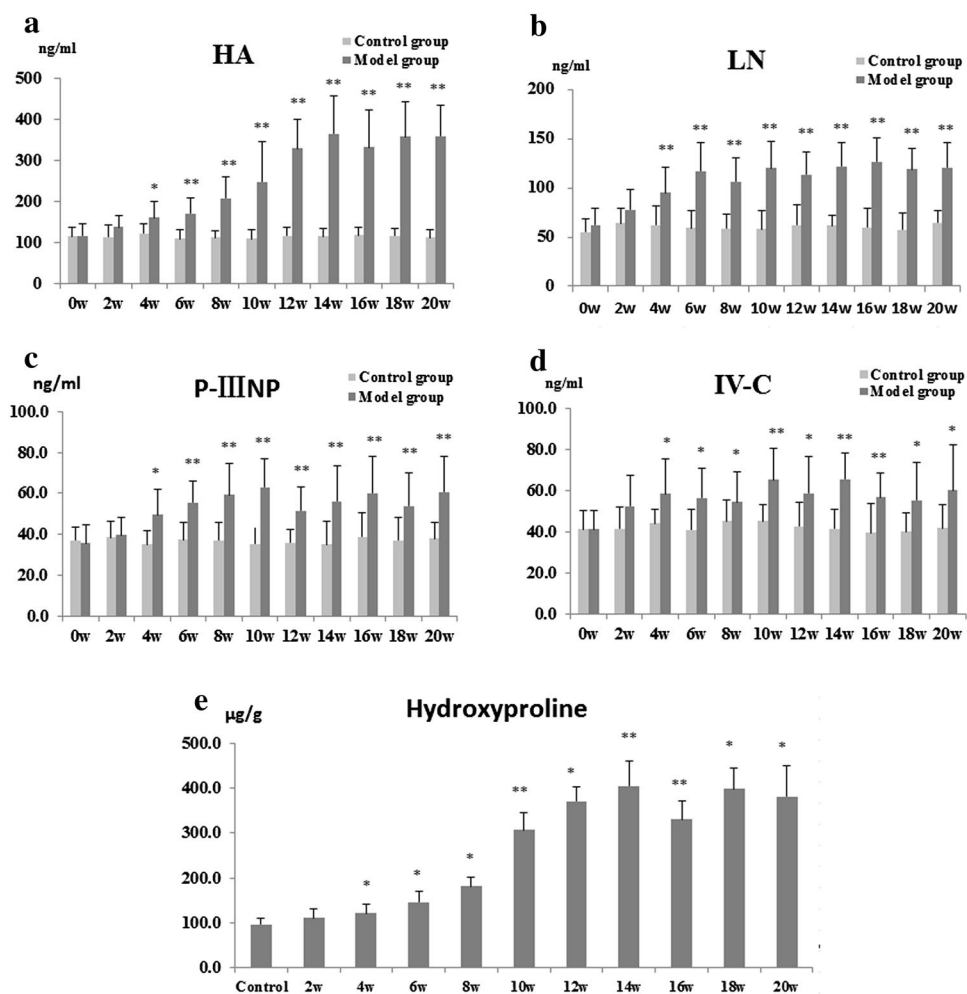


**Fig. 5** Representative results of liver nodules on T2-weighted image. MRI was performed at week 16, week 18 and week 20. Multiple nodules appeared

### Results of histopathological examination

The hepatic histological sections from control rats displayed the normal hepatic lobules organization, normal hepatocytes and sinusoidal architecture. As expected, no tumors were observed in control group (Fig. 6a). The inflammation, fibrosis and HCC in DEN treatment group appeared one after another from the beginning of DEN

injection. Rats in DEN-treated group by week 6 showed fat droplet deposition in hepatocytes, disordered lobular structure, broadly distributed edematous lobular hepatic cells, a large amount of lipid vacuoles formed, obvious inflammatory cell infiltration and a little of collagen fibers (Fig. 6a, b, week 2–6). A significant improvement in inflammation grade was observed after DEN injection (Table 3). 100% of five rats developed A3 (severe activity) grade by week

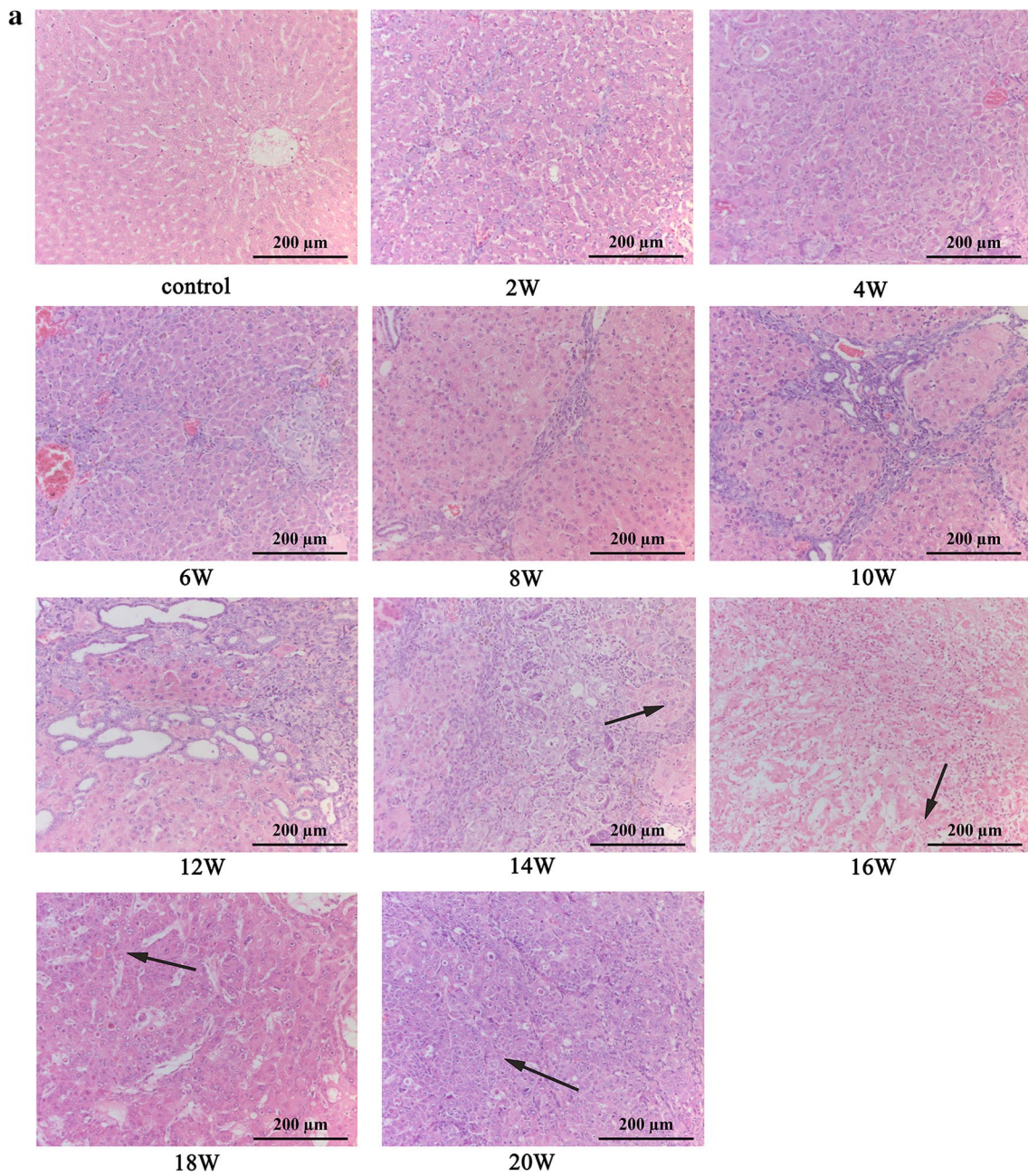


**Fig. 6** Examination of liver histology after DEN induced on hepatic inflammation-fibrosis-cancer axis. Representative photomicrographs of HE (a) and Masson staining (b) at 2–20 weeks (×200); Arrows indicate the representative tumors

6. Week 2–6 was the characteristic histological changes of inflammation, and was called inflammation stage.

DEN treatment for 12 weeks, microscopic fibrosis became obvious and distinct cirrhosis appeared, as indicated by Masson staining. More advanced hepatic fibrosis and regenerating lobules were often observed. The collagen was mainly deposited perilobularly. Hemorrhagic necrosis with foci of lymphomonocytic infiltration around fibrosis tissue can be seen (Fig. 6a, b, week 8–12). We assessed five animals in week 12 and obtained similar results in each

animal. All rats developed F4 grade (cirrhosis) by week 12 according to METAVIR scoring system (Table 4). So the time point of week 8–12 was called fibrosis stage. Week 8 was the time point that was between inflammation and fibrosis stages with mixed features depending on the individual animals.

Subsequent liver fibrosis, there was a marked increase in the incidence of tumors. All the rats in model group developed HCC by week 20. Multiple white nodules were macroscopically observed on the surface of the livers

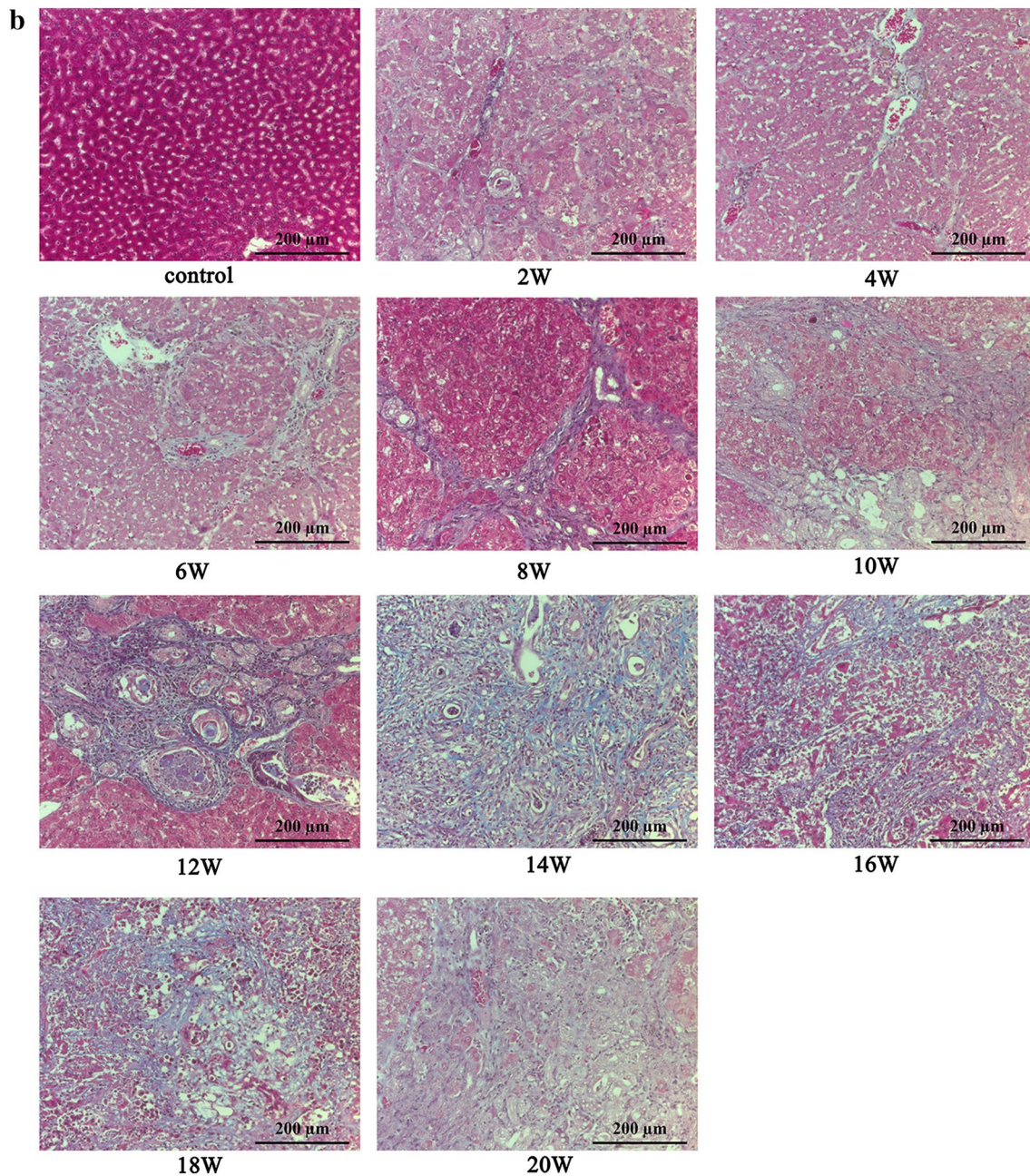


**Fig. 6** (continued)

treated with DEN. The white nodules were demonstrated to be HCC in the histological analysis. The tumor cells had clear, eosinophilic or hyper basophilic cytoplasm, and all had enlarged and hyperchromatic nuclei (Fig. 6a, b, week 14–20). These appearances showed the HCC with various grades of differentiation. Week 14–20 was called HCC stage. Week 14 was the time point that was between fibrosis and HCC stages with mixed features depending on the individual animals.

In summary, all surviving animals from DEN group appeared hepatocellular carcinoma at the end of the experiment. The development of this HCC animal model was divided into three stages: the inflammation stage (week 2–6), the fibrosis stage (week 8–12), and the HCC stage (week 14–20). Week 8 and week 14 were the points of time between two stages with mixer features.



**Table 3** Inflammation stages of rats treated with diethylnitrosamine assessed by METAVIR score

Time	A0	A1	A2	A3	P value (vs control)
Control (n = 10)	10 (100%)	0 (0%)	0 (0%)	0 (0%)	
2 weeks (n = 5)	0 (0%)	5 (100%)	0 (0%)	0 (0%)	0.001
4 weeks (n = 5)	0 (0%)	1 (20%)	4 (80%)	0 (0%)	0.001
6 weeks (n = 5)	0 (0%)	0 (0%)	0 (60%)	5 (100%)	0.001
8 weeks (n = 5)	0 (0%)	0 (0%)	0 (0%)	5 (100%)	0.001
10 weeks (n = 5)	0 (0%)	0 (0%)	0 (0%)	5 (100%)	0.001
12 weeks (n = 5)	0 (0%)	0 (0%)	0 (0%)	5 (100%)	0.001
14 weeks (n = 5)	0 (0%)	0 (0%)	0 (0%)	5 (100%)	0.001
16 weeks (n = 5)	0 (0%)	0 (0%)	0 (0%)	5 (100%)	0.001
18 weeks (n = 5)	0 (0%)	0 (0%)	0 (0%)	5 (100%)	0.001
20 weeks (n = 11)	0 (0%)	0 (0%)	0 (0%)	11 (100%)	0.001

Compared to control group; calculated using the Chi-square test

**Table 4** Fibrosis stages of rats treated with diethylnitrosamine assessed by METAVIR score

Time	F0	F1	F2	F3	F4	P value (vs control)
Control (n = 10)	10 (100%)	0 (0%)	0 (0%)	0 (0%)	0 (0%)	
2 weeks (n = 5)	0 (0%)	5 (100%)	0 (0%)	0 (0%)	0 (0%)	0.001
4 weeks (n = 5)	0 (0%)	3 (60%)	2 (40%)	0 (0%)	0 (0%)	0.001
6 weeks (n = 5)	0 (0%)	0 (0%)	5 (100%)	0 (0%)	0 (0%)	0.001
8 weeks (n = 5)	0 (0%)	0 (0%)	2 (40%)	2 (40%)	1 (20%)	0.001
10 weeks (n = 5)	0 (0%)	0 (0%)	0 (0%)	4 (80%)	1 (20%)	0.001
12 weeks (n = 5)	0 (0%)	0 (0%)	0 (0%)	0 (0%)	5 (100%)	0.001
14 weeks (n = 5)	0 (0%)	0 (0%)	0 (0%)	0 (0%)	5 (100%)	0.001
16 weeks (n = 5)	0 (0%)	0 (0%)	0 (0%)	0 (0%)	5 (100%)	0.001
18 weeks (n = 5)	0 (0%)	0 (0%)	0 (0%)	0 (0%)	5 (100%)	0.001
20 weeks (n = 11)	0 (0%)	0 (0%)	0 (0%)	0 (0%)	11 (100%)	0.001

Compared to control group; calculated using the Chi-square test

**The expression of TGF-β1 and α-SMA**

TGF-β represents an important link between fibrosis and neoplasia in the liver by acting as a pro-fibrogenic factor (Bissell 2001). The overexpression of hepatic TGF-β1 was found in HCC tissues and correlated with carcinogenesis, progression and prognosis of HCC. The expression of TGF-β1 in the liver among the treatment group and control group were examined. Immunohistochemical analysis revealed that TGF-β1-positive cells were scarcely observed in the control livers without DEN treatment (Fig. 7a). Following treatment with DEN, the number of TGF-β1-positive cells was significantly increased in the model rats. The result of TGF-β1 was demonstrated by western blotting (Fig. 7b). The expression of TGF-β1 in DEN-treated group was higher than that in control group.

The activated hepatic stellate cells (HSCs) promote HCC growth and invasiveness. As the marker of activated HSCs, the expression of α-SMA in liver tissues from model and control groups was detected by immunohistochemical staining. Positive staining for α-SMA in control tissue was mainly observed in vascular smooth muscle cells and extremely few in perisinusoidal spaces. High quantitative expression of α-SMA was revealed from inflammation stage (Fig. 7a, 6w). There were also lots of α-SMA-positive cells within the carcinomatous nodules and the adjacent non-tumorous tissues in HCC stage (Fig. 7a, 20w). As demonstrated by western blotting, the expression levels of α-SMA in the DEN treated livers were higher than that in control livers (Fig. 7b).

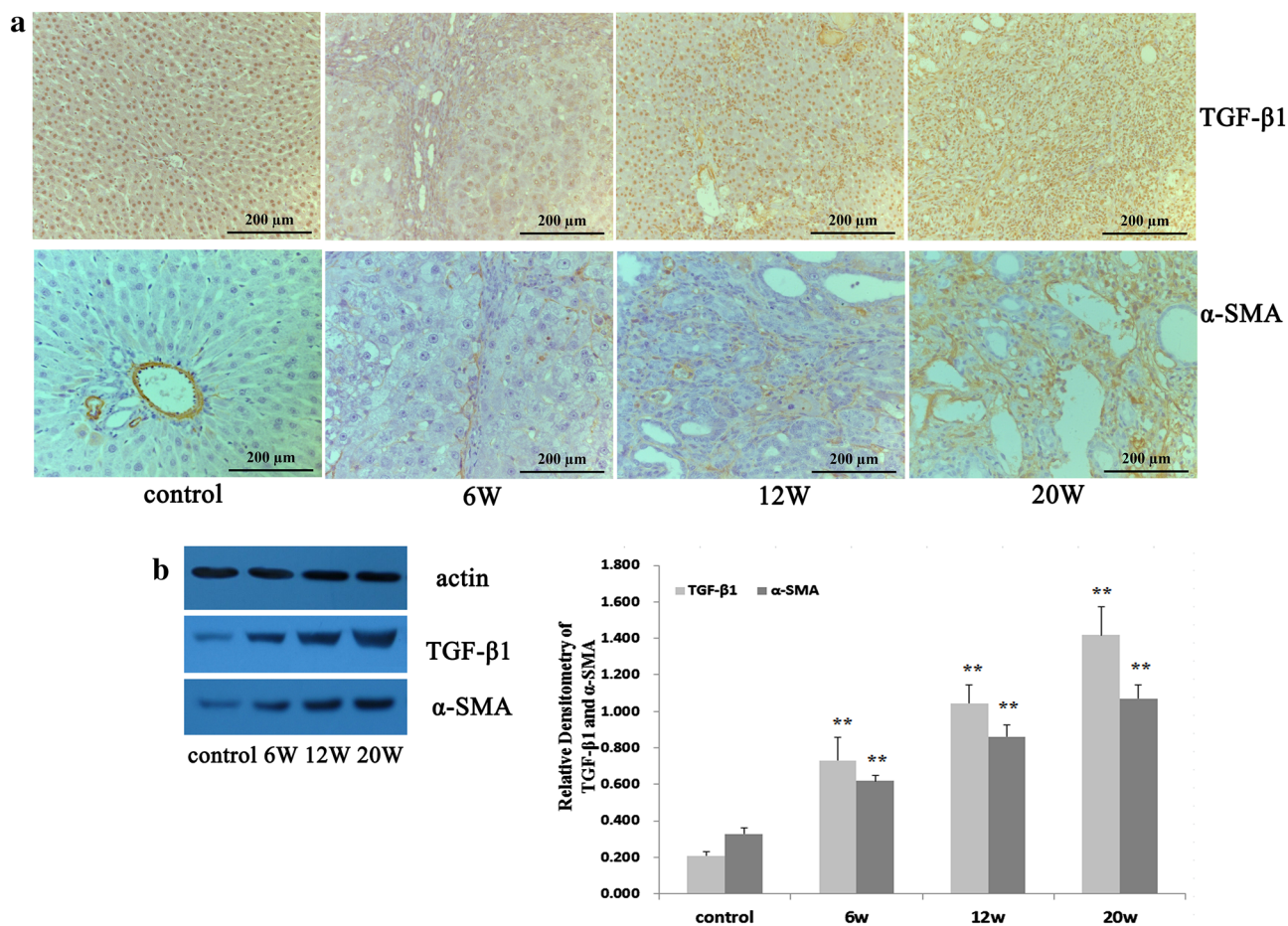


**Fig. 7** Expression of TGF-β1 and α-SMA in the livers of model rats. Expression levels were evaluated by immunohistochemical (a) and western blot analyses (b). a Representative liver tissues immunostained

(×200) with anti-TGF-β1 and α-SMA antibody in control, diethylnitrosamine treated for 6, 12 and 20 weeks. b Hepatic expression of TGF-β1 and α-SMA by western blotting

## Results of PCR

Following DEN exposure, there was a marked increase in inflammatory cytokines, IL-6 and TNF-α. The hepatic tissue of DEN-treated rats had an increased IL-6 and TNF-α mRNA levels in comparing to the control group ( $P < 0.05$ – $0.01$ , Fig. 8a). The expression levels in the model group appeared significant differences with the control group from week 2 and remained at a high levels until the end of the study.

Collagen I and collagen III are the markers of liver fibrosis and its expression is a useful tool for the development of liver fibrosis and hepatic carcinoma. When compared to that of control group, rats of the DEN-treated group were suffered from the significant increase of collagen I and collagen III mRNA levels in the livers at time points of week 4 to week 20 ( $P < 0.01$ , Fig. 8c).

## Up-regulation of JAK2/STAT3 signaling

The Janus kinase (JAK)-signal transducer and activator transcription factor (STAT) signaling pathway is known to be a major cascade associated with the signal transduction for many cytokines and growth factors. The activation of JAK and STAT depends on the phosphorylation at the specific tyrosine residues. IL-6 stimulation leads to the phosphorylation of JAK2, followed by nuclear translocation of the STAT3 homodimer (Zhao et al. 2015; Ma et al. 2016). With ELISA and PCR, we found that IL-6 was up-regulated in DEN-treated rats throughout the experimental period. To elucidate the underlying molecular mechanism of HCC, we identified JAK2/STAT3 as a candidate. So next we sought to examine the JAK2/STAT3 signaling pathway in liver tissues which treated by DEN. We found that JAK2 was significantly increased compared to that in control

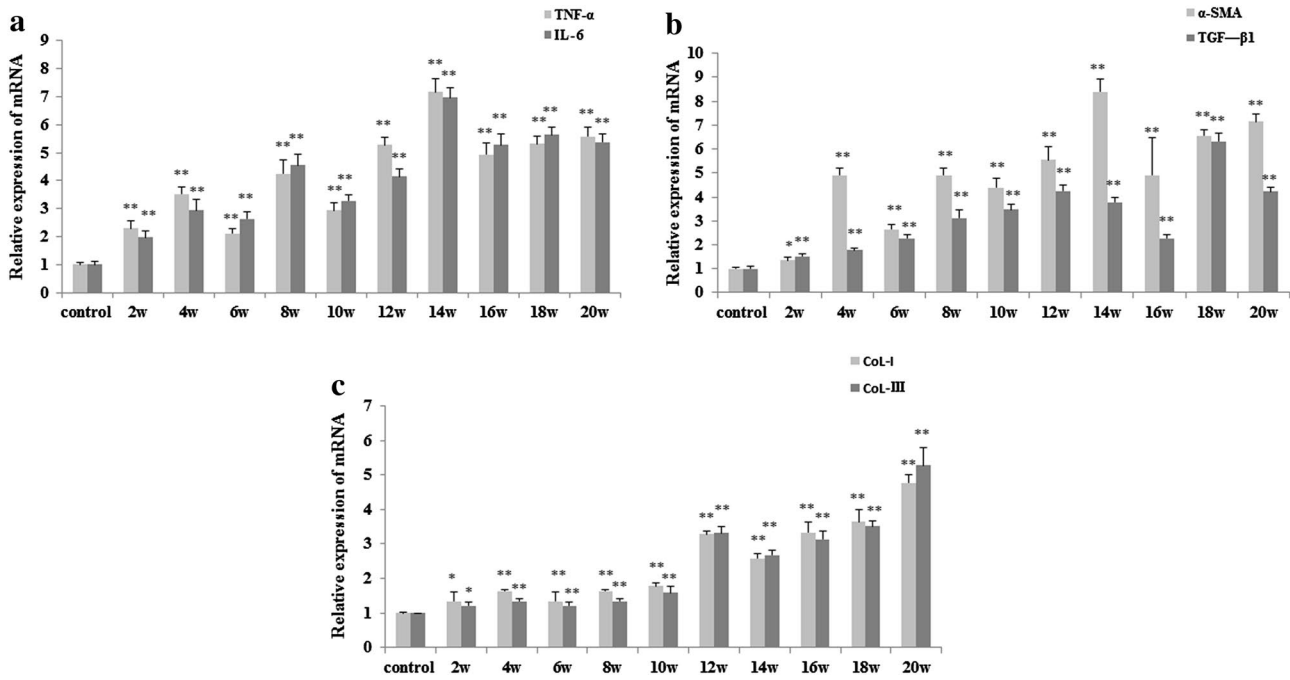


**Fig. 8** Expression of IL-6, TNF- $\alpha$ ,  $\alpha$ -SMA, TGF- $\beta$ 1, collagen I and collagen III in the livers of DEN-treated rats. Real-time PCR analyses of IL-6 and TNF- $\alpha$  (a),  $\alpha$ -SMA and TGF- $\beta$ 1 (b), collagen I and col-

lagen III (c). Results are expressed as mean  $\pm$  SD ( $n=3$ ). \* $P<0.05$ , \*\* $P<0.01$  vs control group

group (Fig. 9). Using western blotting, we also observed that STAT3 and phosphorylation of STAT3 (P-STAT3) were up-regulated as shown in Fig. 9. The effect on JAK2/STAT3 was time dependent.

### Discussion

HCC is a leading cause of morbidity and mortality. In this study, we aimed to analyze the development features of hepatocellular carcinoma. The DEN model for this study is a pre-clinical model of hepatocellular cancer that exhibits many phenotypic characteristics relevant to the liver cancer. Treatment of DEN usually gives rise to stepwise hepatic necroinflammation and liver fibrogenesis followed by the appearance of low- and high-grade dysplastic nodules. (Borbath and Stärkel 2011; Calès et al. 2010; Aravalli et al. 2013). Our model resulted in liver carcinoma within 20 weeks induced by DEN. Since the first documented proposition of an association between inflammation and cancer by the German pathologist Rudolf Virchow in the mid-nineteenth century, our understanding of inflammation and cancer has improved dramatically (Di Virgilio 2014; Kong et al. 2016). However, the underlying molecular mechanisms that are responsible for the high rate of HCC development in the chronically injured and fibrotic liver remain largely unknown and the understanding of HCC

pathogenesis is incomplete. Inflammation-fibrosis-cancer (IFC) axis was proposed and gradually attracted the attention of scholars.

In our study, the model of hepatocellular carcinoma was induced by DEN in which DNA damage contributes to necrotic cell death, resulting in an inflammatory reaction that promotes tumor development. Inflammation is not only being a tumor initiator but also a tumor promoter (Grivennikov et al. 2010). Inflammatory processes are involved in triggering the molecular and cellular events leading from liver injury to fibrosis and ultimately to HCC. Activation of macrophages and neutrophils, as well as the resultant release of pro-inflammatory cytokines and chemokines (IL-6, IL-8, IL-1 $\beta$ , TNF- $\alpha$ , CCL2, CCL20), is thought to play an important role in the pathogenesis of human liver cancer (Uehara et al. 2014). In our study, the concentrations of IL-6 and TNF- $\alpha$  in serum and liver were higher than control group from week 2 and at a high levels all the time. We also found that IL-6/JAK2/STAT3 signaling was activated and the levels of JAK2, STAT3 and P-STAT were up-regulated. It is of note that the occurrence of HCC may be suppressed by reducing the degree of inflammation. According to the histopathological features study at the beginning of DEN-treated, fat droplets occupied the cytoplasm of hepatocytes, pushing the nucleus to the periphery, and the cytoplasm of hepatocytes is filled with tiny lipid droplets. Inflammation also appeared, and consisted of a

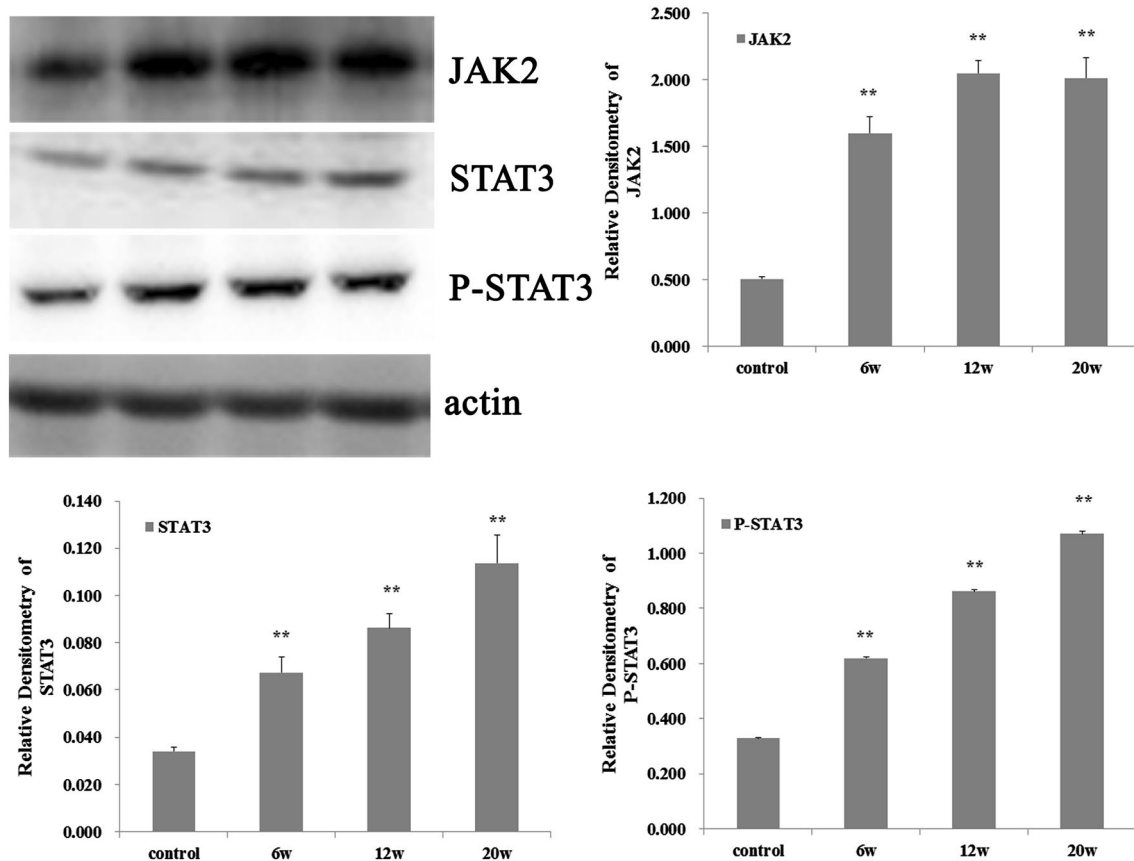


**Fig. 9** Up-regulation of JAK2/STAT3 signaling in the liver of DEN-treated livers. Western blotting analyses of JAK2/STAT3 signaling

mixed inflammatory cell infiltrated (lymphocytes, neutrophils, eosinophils, and Kupffer cells) (Takahashi and Fukusato 2014). These features were mainly found from week 2 to week 6 after the DEN treated in our study, and this time point was called inflammation stage. This result consists with present research (Uehara et al. 2014; Duan et al. 2014).

Followed the inflammatory response, fibrosis gradually appeared and became the main pathological features (Tachi et al. 2015). Advanced inflammation, repeated dosing of DEN leads to progressively worsening pathological changes, liver fibrosis/ cirrhosis. The long-term follow-up study found that progressive fibrosis was significantly correlated with the development of HCC in patients. According to an epidemiological survey, 70–90% of clinical HCC cases are associated with advanced liver fibrosis or cirrhosis (Wong and Janssen 2015; Farazi and Depinho 2006). In our study, the model shows that 100% of the animals in the treatment group developed chronic liver fibrosis at week 12. The levels of Collagen I and Collagen III mRNA in DEN-treated group were higher than those from the control group. Masson staining showed that more and more collagen deposited from week 8 to week 12, and it is the fibrosis

stage in the development of HCC. Given the importance of liver fibrosis/cirrhosis in the process of human HCC, integrative studies that evaluate the mechanisms of fibrogenesis, and how they relate to hepatocyte transformation and modulation of oncogenic signaling, are most relevant to better understanding of the pathogenesis of human disease.

By treated with DEN, our model resulted in carcinoma within 20 weeks. Sustain exposure to DEN caused accumulated extra reactive oxygen species (ROS), in hepatic cells. Excessive concentration of ROS may trigger different reactions concerning oxidative cell defense, which may hamper the definition of a cell profile response. The balance between ROS production and antioxidant capability was disturbed, resulting in oxidative stress and DNA damage in hepatocytes, and finally triggering liver carcinogenesis (Geiger-Maor et al. 2015; Kishida et al. 2016; Santos et al. 2014). The resultant chronic inflammation and fibrosis are accompanied by a dramatic increase in the liver tumor incidence. The histological examination confirmed that the hepatocarcinogenesis model was successfully established, and 100% of the animals in the DEN-exposed group developed liver tumors at 20 weeks in our study. The histopathological features of this HCC model consist of

a broad trabecular growth pattern of atypical hepatocytes with hemorrhaging and ischemic necrosis in the center of the tumors. This model displays proliferation of relatively uniform hepatocytes accompanied with loss of normal lobular architecture and compression of the surrounding parenchyma. So far, the liver had experienced inflammation stage, fibrosis stage, and finally into liver cancer. Thus the histopathological features observed in this model are similar to human HCC.

In conclusion, based on IFC axis, the sequence development of hepatic tumorigenesis was studied following treatment with a carcinogen (DEN). The relative indexed of inflammation, fibrosis, and HCC were detected. Time series specimens from this animal model were analyzed to reveal the specific time points of different stages. The model characterized in our protocol resulted in three stages: the inflammation stage (week 2–6), the fibrosis stage (week 8–12), and the HCC stage (week 14–20). Compared with previous reports, this dynamic study of the stepwise hepatocarcinogenesis process would prefer to the screening of early biomarkers of HCC. This analysis might help elucidate molecular events associated with early and late events in HCC development and progression. In addition, the present work also provides useful clues for future mechanism exploration and identification of therapeutic targets of HCC.

#### Compliance with ethical standards

**Conflict of interest** The author(s) declare(s) that they have no conflicts of interest to disclose.

**Funding** This study was supported by a Grant from the National Natural Science Foundation of China (Nos. 81373888, 81102884).

**Ethical approval** This study was approved by the Animal Experimental Ethical Committee of Jiangsu Province Academy of Traditional Chinese Medicine.

#### References

- Aravalli RN, Cressman EN, Steer CJ (2013) Cellular and molecular mechanisms of hepatocellular carcinoma: an update. *Arch Toxicol* 87:227–247. doi:10.1007/s00204-012-0931-2
- Bissell DM (2001) Chronic liver injury, TGF- $\beta$  and cancer. *Exp Mol Med* 33:179–190
- Borbath I, Stärkel P (2011) Chemoprevention of hepatocellular carcinoma. Proof of concept in animal models. *Acta Gastroenterol Belg* 74:34–44
- Calès P, Boursier J, Chaigneau J et al (2010) Diagnosis of different liver fibrosis characteristics by blood tests in non-alcoholic fatty liver disease. *Liver Int* 30:1346–1354
- Costentin CE, Roudot-Thraval F, Zafrani ES et al (2011) Association of caffeine intake and histological features of chronic hepatitis C. *J Hepatol* 54:1123–1129
- Cubero FJ (2016) Shutting off inflammation: a novel switch on hepatic stellate cells. *Hepatology* 63:1086–1089
- Di Virgilio F (2014) Purinergic receptors in cancer and inflammation: from Rudolph Virchow to Geoff Burnstock. *Purinergic signalling*, vol 10. Springer, Netherlands, pp 657–658
- Ding Y, Peng Y, Li J et al (2013) Gualou Xiebai Decoction prevents myocardial fibrosis by blocking TGF-beta/Smad signalling. *J Pharm Pharmacol* 65:1373–1381
- Duan XY, Pan Q, Yan SY et al (2014) High-saturate-fat diet delays initiation of diethylnitrosamine-induced hepatocellular carcinoma. *BMC Gastroenterol* 14:195. doi:10.1186/s12876-014-0195-9
- Elsharkawy AM, Mann DA (2007) Nuclear factor-kappaB and the hepatic inflammation-fibrosis-cancer axis. *Hepatology* 46:590–597.
- Farazi PA, Depinho RA (2006) Hepatocellular carcinoma pathogenesis: from genes to environment. *Nat Rev Cancer* 6:674–687
- Geiger-Maor A, Guedj A, Even-Ram S (2015) Macrophages regulate the systemic response to DNA damage by a cell nonautonomous mechanism. *Cancer Res* 75:2663–2673. doi:10.1158/0008-5472.CAN-14-3635
- Grivennikov SI, Greten FR, Karin M (2010) Immunity, inflammation, and cancer. *Cell* 140:883–899
- Hernandez-Gea V, Toffanin S, Friedman SL et al (2013) Role of the microenvironment in the pathogenesis and treatment of hepatocellular carcinoma. *Gastroenterology* 144:512–527
- Kishida N, Matsuda S, Itano O (2016) Development of a novel mouse model of hepatocellular carcinoma with nonalcoholic steatohepatitis using a high-fat, choline-deficient diet and intraperitoneal injection of diethylnitrosamine. *BMC Gastroenterol* 16:61. doi:10.1186/s12876-016-0477-5
- Knodell RG, Ishak KG, Black WC et al (1981) Formulation and application of a numerical scoring system for assessing histological activity in asymptomatic chronic active hepatitis. *Hepatology* 1:431–435
- Kong L, Zhou Y, Bu H et al (2016) Deletion of interleukin-6 in monocytes/macrophages suppresses the initiation of hepatocellular carcinoma in mice. *J Exp Clin Cancer Res* 35:131. doi:10.1186/s13046-016-0412-1
- Li J, Sun Z, Zhang J et al (2011) A dual-targeting anticancer approach: soil and seed principle. *Radiology* 260:799–807
- Li C, Bi X, Huang Y et al (2014) Variants identified by hepatocellular carcinoma and chronic hepatitis B virus infection susceptibility GWAS associated with survival in HBV-related hepatocellular carcinoma. *PLoS One* 9(7):e101586. doi:10.1371/journal.pone.0101586
- Ma W, Sze KM, Chan LK et al (2016) RhoE/ROCK regulates chemoresistance through NF-KB/IL-6/STAT3 signaling in hepatocellular carcinoma. *Oncotarget* 27:41445–41459. doi:10.18632/oncotarget.9441
- Peng Y, Ding Y (2015) Pharmacokinetics and tissue distribution study of caudatin in normal and diethylnitrosamine-induced hepatocellular carcinoma model rats. *Molecules* 20:4225–4237
- Santos NP, Colaco A, da Costa R M G (2014) *N*-diethylnitrosamine mouse hepatotoxicity: time-related effects on histology and oxidative stress. *Exp Toxicol Pathol* 66:429–436
- Tachi Y, Hirai T, Miyata A et al (2015) Progressive fibrosis significantly correlates with hepatocellular carcinoma in patients with a sustained virological response. *Hepatol Res* 45:238–246. doi:10.1111/hepr.12331
- Takahashi Y, Fukusato T (2014) Histopathology of nonalcoholic fatty liver disease/nonalcoholic steatohepatitis. *World J Gastroenterol* 20:15539–15548. doi:10.3748/wjg.v20.i42.15539
- Tyler PD, Mcdevitt JL, Sheu AY et al (2013) Seven-tesla magnetic resonance imaging accurately quantifies intratumoral uptake of therapeutic nanoparticles in the McA rat model of hepatocellular

- carcinoma: preclinical study in a rodent model. *Investig Radiol* 49:87–92
- Uehara T, Pogribny I P, Rusyn I (2014) The DEN and CCl<sub>4</sub>-induced mouse model of fibrosis and inflammation-associated hepatocellular carcinoma. *Curr Protoc Pharmacol* 66:14.30.1–14.30.10
- Wong WS, Janssen H L A (2015) Can we use HCC risk scores to individualize surveillance in chronic hepatitis B infection? *J Hepatol* 63:722–732
- Zeng J, Huang X, Zhou L et al (2015) Metabomics identifies biomarker pattern for early diagnosis of hepatocellular carcinoma: from diethylnitrosamine treated rats to patients. *Sci Rep* 5:16101. doi:[10.1038/srep16101](https://doi.org/10.1038/srep16101).
- Zhao H, Guo Y, Han R et al (2015) A novel anti-cancer agent Icaritin suppresses hepatocellular carcinoma initiation and malignant growth through the IL-6/Jak2/Stat3 pathway. *Oncotarget* 31:31927–31943. doi:[10.18632/oncotarget.5578](https://doi.org/10.18632/oncotarget.5578)